A NEW WEIGHTED ANISOTROPIC TOTAL VARIATION ALGORITHM FOR LIMITED ANGLE TOMOGRAPHY

Y. Huang[⋆], *O. Taubmann*[⋆‡], *X. Huang*[⋆], *V. Haase*[∗], *G. Lauritsch*[†], *A. Maier*[⋆‡]

[⋆]Friedrich-Alexander-University Erlangen-Nuremberg, Pattern Recognition Lab, Erlangen, Germany
[†]Siemens Healthcare GmbH, Forchheim, Germany
[‡]Erlangen Graduate School in Advanced Optical Technologies (SAOT), Erlangen, Germany
[∗]University of Luebeck, Institute for Signal Processing, Luebeck, Germany

ABSTRACT

This paper addresses streak reduction in limited angle tomography. The weighted total variation (wTV) algorithm is able to remove most Poisson noise and small streaks for clinical limited angle data. However, it is still not sufficient to remove larger streaks whose orientations are mostly dependent on the scan trajectory. We propose a new weighted anisotropic total variation (waTV) algorithm, which uses four neighboring pixels to calculate the gradient along the streaks' normal direction and is able to reduce large streaks well.

***Index Terms*—** Total variation, limited angle tomography, streak artifacts

1. INTRODUCTION

In imaging systems used for computed tomography (CT), the limited angle problem arises when the gantry rotation is restricted by other system parts or scanning time, such that only limited angle data can be acquired. Due to data incompleteness, streak artifacts will occur. Recently, researchers have made efforts on suppressing streak artifacts in insufficient data reconstruction. In this context, compressed sensing technologies attract tremendous attention since they can use relatively few data to obtain a good reconstruction result by exploiting sparsity in a specific domain [1–4]. Particularly, iterative reconstruction algorithms regularized by total variation (TV) minimization were demonstrated to be effective in reducing streak artifacts in limited angle tomography [5].

In limited angle tomography, the shape and orientation of streak artifacts is closely related to the angles missing in the acquisition. Based on this property, Chen et al. [6] developed the anisotropic TV (aTV) by assigning different weighting factors to different directions. The aTV algorithm shows a better performance than isotropic TV in terms of streak artifacts reduction and edge recovery. However, some structures in the clinical reconstructed image may be blurred because of the staircasing effect.

In 2008, Candès et al. [7] proposed the weighted TV (wTV) algorithm to more effectively enhance sparsity in the gradient domain, which can avoid the staircasing effect. In this paper, we investigate the application of wTV on limited angle tomography. Additionally, based on the property of limited angle tomography that the orientations of streak artifacts are mostly dependent on the scan trajectory, a new weighted anisotropic TV (waTV) is proposed, which uses four neighboring pixels instead of two pixels to compute the gradient along the streaks' normal direction.

2. METHODS

The optimization model of the wTV algorithm can be

$$\min_{\boldsymbol{f}} ||\boldsymbol{f}||_{\mathrm{wTV}} \quad \text{subject to} \quad \boldsymbol{A}\boldsymbol{f} = \boldsymbol{p}, \tag{1}$$

where $\boldsymbol{f}$ is the image, $\boldsymbol{A}$ is the system matrix and $\boldsymbol{p}$ is the acquired projection data. $||\boldsymbol{f}||_{\mathrm{wTV}}$ is defined as [7]

$$\begin{aligned} ||\boldsymbol{f}||_{\mathrm{wTV}} &= \sum_{x,y,z} \boldsymbol{W}_{x,y,z} ||\,(\mathcal{D}\boldsymbol{f})_{x,y,z}\,||, \\ \boldsymbol{W}_{x,y,z} &= \frac{1}{||(\mathcal{D}\boldsymbol{f})_{x,y,z}|| + \epsilon}, \end{aligned} \tag{2}$$

where $\boldsymbol{W}$ is the weight matrix, x, y and z are pixel indices and ϵ is a parameter influencing the reconstructed image resolution. $\mathcal{D}\boldsymbol{f}$ is the gradient of the image $\boldsymbol{f}$ defined as

$$(\mathcal{D}\boldsymbol{f})_{x,y,z} = (\mathcal{D}_x\boldsymbol{f}_{x,y,z}, \mathcal{D}_y\boldsymbol{f}_{x,y,z}, \mathcal{D}_z\boldsymbol{f}_{x,y,z}), \tag{3}$$

where $\mathcal{D}_x$, $\mathcal{D}_y$ and $\mathcal{D}_z$ are the discrete gradient operators along the X, Y and Z axes, which are

$$\begin{aligned} \mathcal{D}_x\boldsymbol{f}_{x,y,z} &= \boldsymbol{f}_{x,y,z} - \boldsymbol{f}_{x-1,y,z}, \\ \mathcal{D}_y\boldsymbol{f}_{x,y,z} &= \boldsymbol{f}_{x,y,z} - \boldsymbol{f}_{x,y-1,z}, \\ \mathcal{D}_z\boldsymbol{f}_{x,y,z} &= \boldsymbol{f}_{x,y,z} - \boldsymbol{f}_{x,y,z-1}. \end{aligned} \tag{4}$$

The flow chart of the whole algorithm is shown in Fig. 1. The main loop iterates at most N times and each iteration contains a simultaneous algebraic reconstruction technique

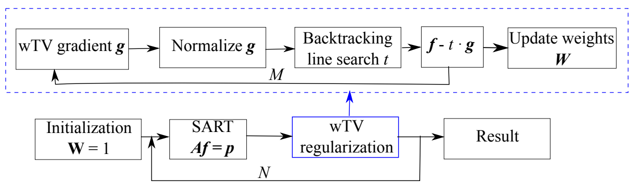

Fig. 1. The wTV algorithm iterates SART and wTV minimization steps alternatively N times in the outer loop and repeats the gradient descent process M times in the inner loop.

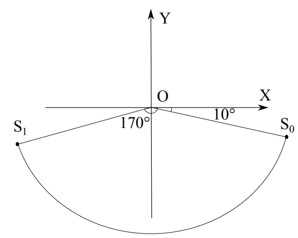

Fig. 2. Scan trajectory.

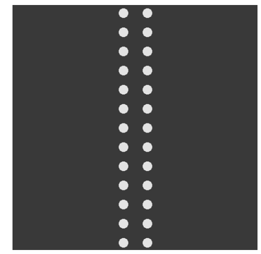

Fig. 3. Numerical phantom, window: [-400 1400] HU.

(SART) [3] step to increase data fidelity and a wTV minimization step for regularization. In each wTV minimization step, we regard the weight matrix $\boldsymbol{W}$ as constant for computing the gradient of $||\boldsymbol{f}||_{\mathrm{wTV}}$ to retain a convex problem [7],

$$\boldsymbol{g}_{x,y,z} = \frac{\partial ||\boldsymbol{f}||_{\mathrm{wTV}}}{\partial \boldsymbol{f}_{x,y,z}}, \tag{5}$$

and repeat the gradient descent process M times with backtracking line search algorithm [8]. After that $\boldsymbol{W}$ is updated.

Since the regular wTV algorithm only uses two neighboring pixels to compute the gradient in each direction, these gradient operators are hardly able to detect variations on a larger scale (Figs. 4(a) and 6(c)). In limited angle reconstruction, orientations of streaks can be aligned with a coordinate axis, e.g. the X-axis, if we choose a proper corresponding scan angle range $10° - 170°$, which means more variations along Y direction than X and Z directions. Therefore, we want to enforce homogeneity more strongly in the Y direction. Aiming at this, we propose the waTV algorithm by replacing $\mathcal{D}\boldsymbol{f}$ with an anisotropic variant. Specifically, while $\mathcal{D}_x\boldsymbol{f}$ and $\mathcal{D}_z\boldsymbol{f}$ are kept the same as those in Eqn. 4, we use four neighboring pixels to compute a modified Y-gradient estimate $\tilde{\mathcal{D}}_y\boldsymbol{f}$,

$$\tilde{\mathcal{D}}_y\boldsymbol{f}_{x,y,z} = a\boldsymbol{f}_{x,y+1,z} + b\boldsymbol{f}_{x,y,z} - b\boldsymbol{f}_{x,y-1,z} - a\boldsymbol{f}_{x,y-2,z}, \tag{6}$$

where a and b are weighting coefficients. The waTV algorithm also follows the framework shown in Fig. 1.

3. EXPERIMENTS

3.1. Numerical phantom

In order to validate the advantage of our proposed waTV algorithm in reducing large horizontal streaks, a 2-D numerical phantom is designed (Fig. 3). The phantom contains two columns of circular areas. The attenuation coefficient for the circular areas is 1200 HU while it is 0 HU for the background. Regarding the acquisition parameters, the scan angle ranges from $10°$ to $170°$ and the angular increment is $1°$. The detector size is 768 pixels and the pixel size is 1 mm. The source to detector distance is $d = 2175$ mm, and the fan angle is $\gamma_{\max} = 20°$. The whole experimental setup, including generation of the phantoms, is implemented in CONRAD [9].

The wTV algorithm and the waTV algorithm are employed to reconstruct this phantom from limited angle data. The coefficients $a = b = 1$ as well as $a = 1$, $b = 2$ are evaluated in Eqn. 6 for the waTV algorithm. All images are reconstructed with $\epsilon = 0.001$ in Eqn. 2 and $M = 10$ chosen heuristically. The reconstruction algorithms stop when they reach the termination criteria $\sigma < 8.0 \cdot 10^{-3}$ HU or $n = 500$, where σ is the root-mean-square difference of two consecutive iteration results and n is the iteration number.

3.2. Clinical data

The wTV algorithm and the waTV algorithm are also compared in a 3-D clinical head dataset acquired with a Siemens Artis zee angiographic C-arm system (Siemens Healthcare GmbH, Forchheim, Germany). The detector size is 1240×960, and the detector pixel size is 0.308 mm. The complete data contains 496 projections obtained in a $200°$ short scan. We simulate a limited angle acquisition with a scan angle from $10°$ to $170°$ where only the projections 25 through 422 are used. The reconstruction image grid size is $512 \times 512 \times 256$, and the pixel sizes are 0.4 mm, 0.4 mm and 0.8 mm in X, Y and Z direction, respectively.

We first use SART and wTV to reconstruct the complete data as an image quality reference. The fine bony structures and soft brain tissues can be used to test the reconstruction resolution and contrast. Then wTV and waTV are applied to the limited angle data. During the experiments, we found that it is beneficial to perform 30 SART iterations without regularization first as initialization and then 50 additional iterations of wTV or waTV are carried out.

4. RESULTS AND DISCUSSION

The reconstruction results of the numerical phantom are shown in Fig. 4. Comparing Fig. 4(b) with Fig. 4(a), streaks are reduced faster with waTV than with wTV and the plot of the root-mean-square error (RMSE) over iterations (Fig. 4(g)) demonstrates this as well. After around 500 iterations, almost no streaks exist in the image reconstructed by waTV (Fig. 4(d)) while there are still pronounced large streaks in the image reconstructed by wTV (Fig. 4(c)).

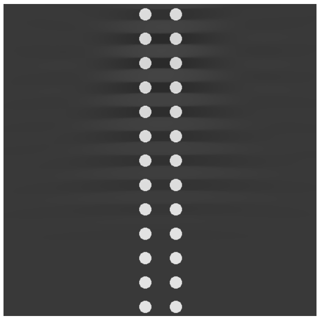

(a) wTV, 250th iteration

RMSE $= 24.40$ HU

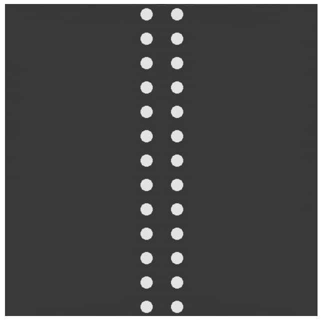

(b) waTV, 250th iteration

$a = b = 1$, RMSE $= 4.96$ HU

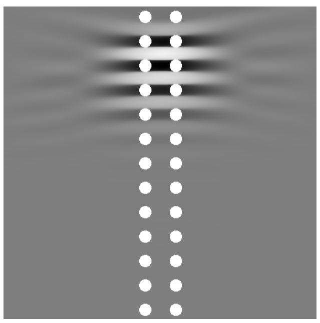

(c) wTV, 500th iteration

RMSE $= 3.75$ HU

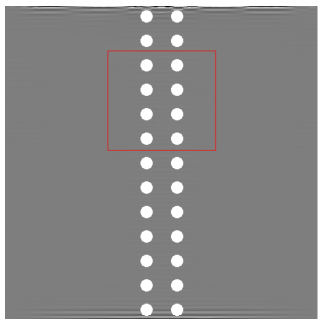

(d) waTV, 497th (final) iteration

$a = b = 1$, RMSE $= 4.16$ HU

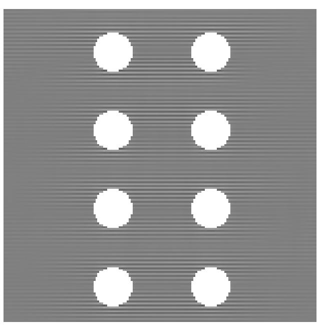

(e) waTV, ROI, $a = b = 1$

RMSE $= 4.16$ HU

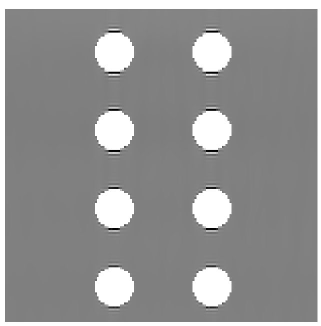

(f) waTV, ROI, $a = 1, b = 2$

RMSE $= 2.56$ HU

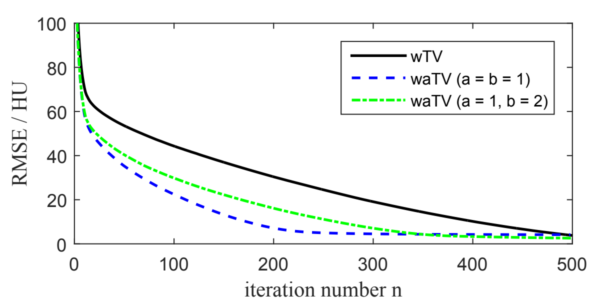

(g) convergence rates of wTV and waTV

Fig. 4. Comparison of wTV and waTV, 500th iteration for (e) and (f), windowing: [-400 1400] HU for (a) and (b), [-24 24] HU for (c) and (d), [-8 8] HU for (e) and (f).

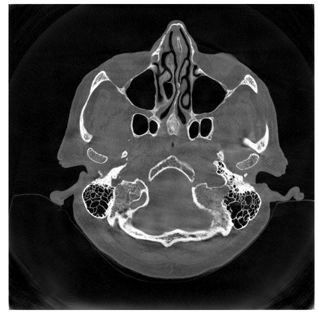

(a) SART, 65th slice

(b) SART, 140th slice

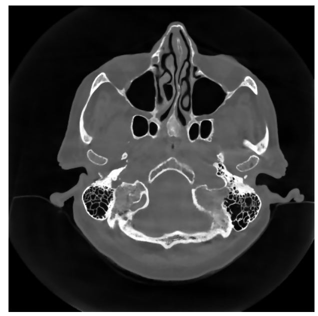

(c) wTV, 65th slice

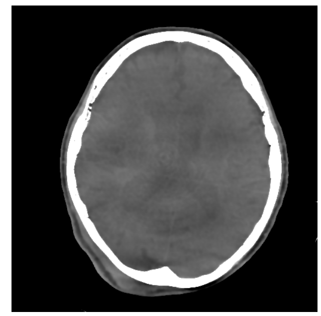

(d) wTV, 140th slice

Fig. 5. Reference images reconstructed from the complete clinical dataset with the SART algorithm and the wTV algorithm. Windowing: [-1000 1730] HU for (a) and (c), [-220 365] HU for (b) and (d).

However, if we choose a narrow intensity window [-24 24] HU, we can see some "zebra crossing"-like artifacts in Fig. 4(d), especially at the top and bottom boundaries. It is because $\tilde{\mathcal{D}}_y \boldsymbol{f}_{x,y,z}$ regards such patterns as homogeneous along Y direction in the case of $a = b = 1$. For instance, considering a sequence of intensity value $\boldsymbol{l} = [0\ 1\ 0\ 1\ 0\ 1\ 0\ 1]$, $\tilde{\mathcal{D}}_y \boldsymbol{l} = [0\ 0\ 0\ 0\ 0]$. Hence, if we choose e.g. $a = 1$ and $b = 2$ instead, the artifacts can be reduced though the reconstructed circular areas still slightly lose resolution (Fig. 4(f)). Due to their better performance, we use these weights ($a = 1, b = 2$) for reconstruction of the clinical dataset.

Reconstructions from the complete clinical dataset are shown in Fig. 5. Fig. 5(c) demonstrates that wTV can preserve the fine bone structures almost as well as SART (Fig. 5(a)). In addition, the brain texture is shown well in the wTV result (Fig. 5(d)) while it is almost totally lost in the noise in the SART result (Fig. 5(c)). This indicates that wTV is an effective denoising tool.

Image results of SART, wTV and waTV for limited angle tomography are shown in Fig. 6. Compared to SART (Figs. 6(a) and 6(b)), wTV (Figs. 6(c) and 6(d)) can remove small streaks well and the bone structures and the brain texture look better than the SART results. However, it is still not able to remove the large scale streaks which are almost along the horizontal direction and some anatomical structures are

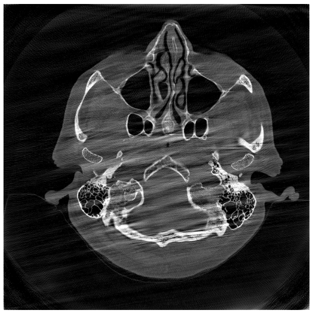

(a) SART as initialization

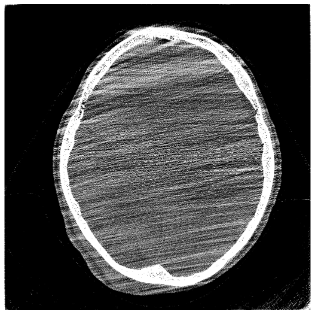

(b) SART as initialization

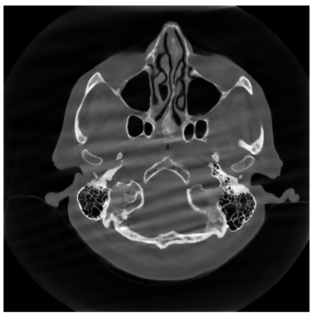

(c) wTV with initialization

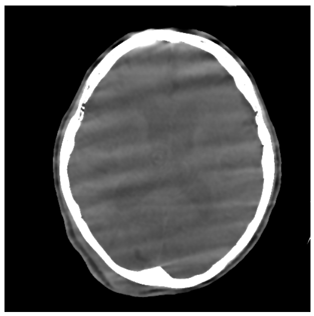

(d) wTV with initialization

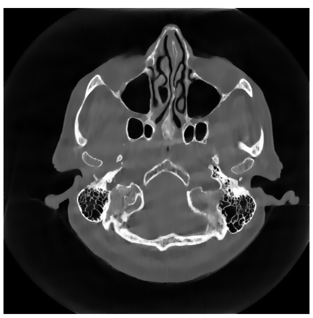

(e) waTV with initialization

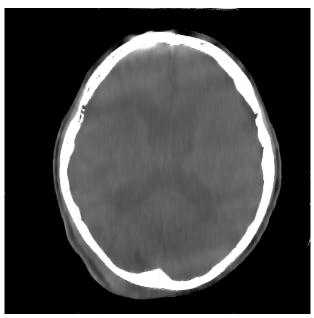

(f) waTV with initialization

Fig. 6. Comparison of SART, wTV and waTV ($a = 1$, $b = 2$) in limited angle tomography. Windowing: [-1000 1730] HU for (a), (c) and (e), [-220 365] HU for (b), (d) and (f).

obscured by them. In contrast, waTV removes small as well as large streaks while preserving both the fine bone structures and the brain texture well. This clinical experiment suggests that waTV is a better choice than wTV w. r. t. streak reduction in limited angle tomography. Still, Fig. 6(f) shows the image reconstructed with waTV may lose some resolution compared to the reference image (Fig. 5(d)).

5. CONCLUSION AND OUTLOOK

From the experiments, we can conclude that wTV is a good denoising method since it can remove Poisson noise and small streaks very well while preserving the image resolution and contrast. However, it is still not sufficient to remove large scale streaks. Our proposed waTV algorithm can reduce these streaks better while similarly preserving the fine bone structures and the brain texture. However, it may produce new artifacts unless the weights are carefully selected and potentially cause a slight loss of resolution. In future work, more quantitative experiments and assessments should be carried out to explore the trade-off between resolution and artifacts reduction. Besides, the effects of various weights as well as various pixel lengths for $\tilde{\mathcal{D}}_y$ in Eqn. 6 should be further investigated.

Disclaimer: The concepts and information presented in this paper are based on research and are not commercially available.

References

[1] E.J. Candès, J. Romberg, and T. Tao, "Robust uncertainty principles: exact signal reconstruction from highly incomplete frequency information," *IEEE Trans Inf Theory*, vol. 52, no. 2, pp. 489–509, 2006.

[2] E.Y. Sidky and Pan X., "Image reconstruction in circular cone-beam computed tomography by constrained, total-variation minimization," *Med Phys*, vol. 53, no. 17, pp. 4777–4807, 2008.

[3] L. Ritschl, F. Bergner, C. Fleischmann, and M. Kachelriess, "Improved total variation-based CT image reconstruction applied to clinical data," *Phys Med Biol*, vol. 56, no. 6, pp. 1545–1561, 2011.

[4] H. Wu, A. Maier, R. Fahrig, and J. Hornegger, "Spatial-temporal total variation regularization (STTVR) for 4D-CT reconstruction," in *Proc of SPIE*, 2012, vol. 8313.

[5] E.Y. Sidky, C.M. Kao, and X. Pan, "Accurate image reconstruction from few-views and limited-angle data in divergent-beam CT," *J Xray Sci Technol*, vol. 14, pp. 119–139, 2006.

[6] Z. Chen, X. Jin, L. Li, and G. Wang, "A limited-angle CT reconstruction method based on anisotropic TV minimization," *Phys Med Biol*, vol. 58, no. 7, pp. 2119–2141, 2013.

[7] E.J. Candès, M.B. Wakin, and S.P. Boyd, "Enhancing sparsity by reweighted l_1 minimization," *J. Fourier Anal. Appl.*, vol. 14, pp. 877–905, 2008.

[8] S. Boyd and L. Vandenberghe, *Convex Optimization*, Cambridge University Press, 2004.

[9] A. Maier, H. Hofmann, M. Berger, P. Fischer, C. Schwemmer, H. Wu, K. Müller, J. Hornegger, J. Choi, C. Riess, A. Keil, and R. Fahrig, "CONRAD - a software framework for cone-beam imaging in radiology," *Med Phys*, vol. 40, no. 11, pp. 111914, 2013.